Surface-Independent Direct-Projected Augmented Reality

Hanhoon Park, Moon-Hyun Lee, Sang-Jun Kim, and Jong-Il Park

Division of Electrical and Computer Engineering,
Hanyang University, Seoul, South Korea
{hanuni, vivendi, markjun}@mr.hanyang.ac.kr,
jipark@hanyang.ac.kr
http://mr.hanyang.ac.kr

Abstract. Some issues on direct-projected augmented reality (DirectAR) are addressed: the projection may be geometrically distorted due to the non-planar surface (geometric distortion); the projection cannot be seen to user as intended because the position of the projector is not the same as that of the user's viewpoint (viewpoint-ignorant projection); the projection may be modulated by surface color (radiometric distortion); the projected area may not have uniform brightness when the projection is obliquely headed for the surface (uneven projection). We propose an integrated framework for handling all the problems. Experimental results demonstrate that the problems unavoidable in surface-independent DirectAR can be successfully resolved.

1 Introduction

Direct-projected augmented reality (hereafter, it is called DirectAR) approaches have been proposed and applied to many applications such as enhancing the face of an actor or changing the color and texture of real objects [12]. Projection made it possible to use 3-D real and large objects as displays [7] and freed from discomforts incidental to wearing a device such as HMD. For instance, surgeons schedule the operation and check up the state of patient while seeing magnetic resonance imaging (MRI) or computed tomography (CT) images. Medical image visualization has been proved to be useful since the methods for 3-D reconstruction and visualization of the MRI or CT images were emerged [1]. However, it is still stressful for surgeons to keep peering at the CRT display or wearing HMD to see the information during operation. By directly projecting the 3-D reconstructed MRI or CT images onto the patient's body, surgeons can be visually assisted in such a way that they can operate and monitor the patient's state simultaneously.

However, DirectAR usually suffers from the following problems: the projection may be geometrically distorted due to the non-planar surface (*geometric distortion*); the projection cannot be seen to user as intended because the position of the projector is not same as that of the user's viewpoint (*viewpoint-ignorant projection*); the projection may be modulated by the surface color (*radiometric distortion*); the projected area may not have uniform brightness when the projection is obliquely headed for the surface (*uneven projection*). Some papers have addressed these problems partially [8, 11]. In this paper, we aim at providing an integrated framework for handling all the problems.

P.J. Narayanan et al. (Eds.): ACCV 2006, LNCS 3852, pp. 892 – 901, 2006.

Recently, multi-projector-based methods have been proposed to resolve the problems such as multi-focal projection [14] and specularity-free projection [15] other than the aforementioned problems. In this paper, we focus only on the problems regarding using a single projector.

2 Method

In this paper, we attempt to provide practical and easy-to-use algorithms coping with the problems of DirectAR. There is still room for improving the accuracy and further exploration.

2.1 Geometric Registration

Geometric registration indicates that projection is exactly overlaid on the surface without distortion. To do so, the projectors should be calibrated and the surface geometry should be known first. We use a modified version of the well-known Zhang's calibration method [6] for calibrating projectors and a linear triangulation method [5] for recovering the geometry of projection surface. The surface is triangularly represented using the recovered points on the surface because the surface is assumed to be piece-wise planar. Finally, the projection images are patch-wise prewarped using homography to be undistorted.

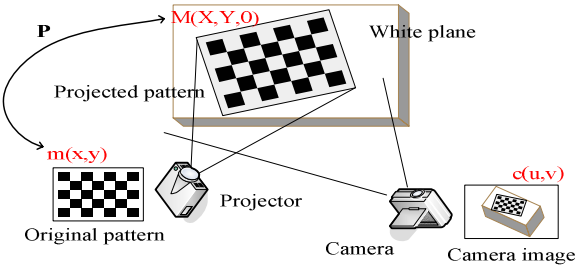

Fig. 1. Projector calibration

2.1.1 Projector Calibration

For calibrating a projector, a modified version of the well-known Zhang's calibration method [6] is used. Coplanar 3-D points and their corresponding 2-D points are required in the Zhang's calibration method. In our method, the points **m**(x,y) on a source pattern of a projector correspond to 2-D points and the projected points **M**$(X,Y,0)$ correspond to 3-D points (see Fig. 1). The coordinates of the projected points are computed from the image captured by a camera as follows[1].

$$\begin{pmatrix} X & Y & 1 \end{pmatrix}^T = H_{c-o}\tilde{c} \tag{1}$$

where H_{c-o} is camera-to-surface homography and $\tilde{c}$ is the homogeneous coordinates of the camera image. The relationship between 3-D points (**M**) and 2-D points (**m**) is represented in homogeneous coordinates as

[1] In this paper, tilde indicates homogenous coordinates.

$$\tilde{m} = P\tilde{M} = H_{o-p}\begin{pmatrix} X & Y & 1 \end{pmatrix}^T \tag{2}$$

where H_{o-p} is surface-to-projector homography. Given the 3-D and 2-D points, optimization algorithms of Zhang's method are used as it is [6].

2.1.2 3-D Surface Modeling

Assuming that the camera and projector are calibrated, a linear triangulation method [5] is used for recovering the geometry of projection surface. The relationship between the coordinates of projection surface, projector coordinates, and camera coordinates is represented as

$$\tilde{m} = P\tilde{M}\ ,\ \tilde{c} = P_c\tilde{M}\ . \tag{3}$$

The homogeneous scale factor is eliminated by a cross product as

$$\tilde{m} \times (P\tilde{M}) = 0\ ,\ \tilde{c} \times (P_c\tilde{M}) = 0 \tag{4}$$

where P_c is camera projection matrix. An equation of the form $AM = 0$ can then be composed, with

$$A = \begin{bmatrix} xp^{3T} - p^{1T} & yp^{3T} - p^{2T} & up_c{}^{3T} - p_c{}^{1T} & vp_c{}^{3T} - p_c{}^{2T} \end{bmatrix}^T \tag{5}$$

where p^{iT} are the rows of P. This is a redundant set of equations, since the solution is determined only up to scale. **A** has a 1-dimensional null-space which provides a solution for **M** and can be computed using Singular Value Decomposition (SVD) [5].

The surface is triangularly represented using the recovered points on the surface because the surface is assumed to be piece-wise planar. In practice, we project a grid pattern onto the surface and compute the 3D coordinates of only the corner points. A dense grid pattern can be used to model the complicated surface.

2.2 Radiometric Compensation

The color of projection is dependent on that of the projection surface. In other words, if the color of the surface is not pure white, the projection is modulated by the color of the surface. The radiometric compensation is a technique that makes the color of projection look unchanged by adjusting the color of the projection in advance when the projection surface has colorful texture. Letting **I** be the projector input image, the projected image $\mathbf{I_P}$ is acquired by projector response function f as

$$I_P = f(I)\,. \tag{6}$$

Thus, the projector input image $\hat{I}$ should be compensated by f^{-1} in advance such that

$$\hat{I} = f^{-1}(I_P)\,. \tag{7}$$

In this paper, the color change of projection is observed by a camera. The compensation result may be incomplete due to the unknown response function of the camera. However, the response function of camera can be easily estimated from multiple images captured with different exposure time [10].

The procedure of radiometric compensation consists of six steps in this paper.

Step 1: The geometric mapping between a projector and a camera is computed. It is explained in Section 2.1.

Step 2: The radiometric model of the pipeline from input projector color to the measured camera color is defined as

$$C = VI_P + F \quad \begin{array}{l} \textit{where C: camera image point} \\ \textit{V: color mixing matrix} \\ \textit{I}_P\textit{: projected image point} \\ \textit{F: ambient light} \end{array} \tag{8}$$

The **V** matrix captures all the coupling between the projector and camera channels and their interactions with the spectral reflectance [4].

Step 3: **F** using black projector image is computed.

Step 4: $\hat{V} = VD^{-1}$ is computed using one reference image and three images which have different values in R, G, B channel, respectively. **D** is the diagonal matrix with diagonal entries of **V** [4]. The recovery of $\hat{V}$ thus allows us to decouple the color channels. It means that $C_k(k$=r,g,b) is determined by only the input brightness of the channel k in Eq. (8). The entries of **D** can be computed from the linear equations which are given by multiplying Eq. (8) by $\hat{V}^{-1}$.

Step 5: The inverse response function f^{-1} of a projector is computed by comparing the 26 projector images with different gray-level i.e. I = 0, 10, 20, …, 250 with the 26 camera images which are acquired by capturing the projector images. f^{-1} is defined as 4th-order polynomial function in this paper because the plot of input projector brightness vs. camera image brightness has the shape as shown in Fig. 2. This computation is performed pixel-wise and channel-wise because each pixel has different response function and each channel also has different response function.

Step 6: The compensated projector input image $\hat{I}$ is computed by Eq. (7).

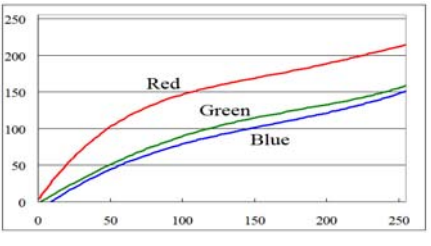

Fig. 2. Plot of projector input brightness (x-axis) vs. camera image brightness (y-axis). The curves are 4th- order approximation.

2.3 Viewer-Dependent Projection

For coping with the user's viewpoint which is tracked using an optical tracker [9] (see Fig. 3), it is assumed that the geometric transformation between user, projectors, and display surface is recovered and 3-D coordinates of the display surface is known. This problem has already been addressed in the previous section.

Figure 3 shows an AR-assistant surgery system [2] as an example of DirectAR system. The system visualizes the 3D position of tumor and additional information on the surface of human body. In the viewpoint of the projector, the direction of the

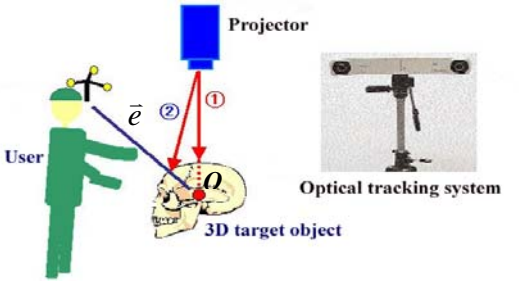

Fig. 3. DirectAR-based surgery system considering user's viewpoint. The graphical contents should be projected to not ① but ②.

projection should be ①. However, it is clear that the direction of the projection should be changed into ② when considering user's viewpoint.

To do so, the intersection point between $\vec{e}$ and the 3-D target object should be estimated. In this paper, a ray/triangle intersection algorithm is used [3]. The algorithm is divided into 2 steps. First, it is estimated if a ray is intersected with a certain triangle. Next, the coordinates of the intersection point is computed.

Step 1: Let V_i for $i \in 0,1,2$ be the coordinates of the three vertices of the triangle. The normal vector of the triangle is represented by

$$\vec{n} = (V_1 - V_0) \times (V_2 - V_0) . \tag{9}$$

Any point V in the triangle's plane satisfies $V \cdot \vec{n}$ + *constant* = 0. The constant d is computed by

$$d = -V_0 \cdot \vec{n} . \tag{10}$$

If a ray parameterized by $O + \vec{e}\, t$ is intersected with a triangle, t parameter is computed by

$$t = (d - \vec{n} \cdot O) / (\vec{n} \cdot \vec{e}) . \tag{11}$$

When $0 \le t \le 1$, the ray intersects with the triangle.

Step 2: A point V in the triangle plane is defined by

$$\overrightarrow{V_0V} = \alpha \overrightarrow{V_0V_1} + \beta \overrightarrow{V_0V_2} \quad \textit{where } \alpha \ge 0, \beta \ge 0, \alpha + \beta \le 1. \tag{12}$$

In the image plane, this can be written as

$$\overrightarrow{v_0v}(u,v) = \alpha \overrightarrow{v_0v_1}(u_1, v_1) + \beta \overrightarrow{v_0v_2}(u_2, v_2) \tag{13}$$

where v_i is an image point of V_i. Therefore, α and β are computed by

$$\alpha = \det\begin{pmatrix} u_0 & u_2 \\ v_0 & v_2 \end{pmatrix} / \det\begin{pmatrix} u_1 & u_2 \\ v_1 & v_2 \end{pmatrix}, \quad \beta = \det\begin{pmatrix} u_1 & u_0 \\ v_1 & v_0 \end{pmatrix} / \det\begin{pmatrix} u_1 & u_2 \\ v_1 & v_2 \end{pmatrix}. \tag{14}$$

After computing the intersection point, the graphical contents are properly pre-warped and projected to the point without geometric distortion.

2.4 Intensity-Compensated Projection

When the projection is obliquely headed for the nonplanar surface, the area of the projection has uneven brightness as shown in Fig. 4. In this paper, we present a geometry-based method for making the projected area have even brightness. The target brightness is obtained by the average brightness of the projection area.

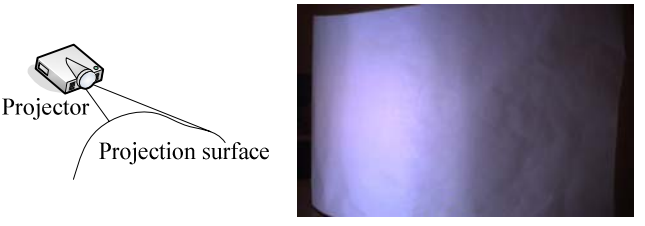

Fig. 4. Uneven projection. The projector lights the nonplanar surface in the left side. The projection is not uniform although an unicolored projection is applied to the surface.

The intensity of projection is dependent on the angle θ between the projection vector and the normal vector (see Fig. 5). The intensity is compensated as follows.

$$\hat{I}_i = wI_i, \quad i = r, g, b. \tag{15}$$

where

$$w = 1 + k_c \sin(\theta - \theta_p) \quad \textit{where } k_c\textit{: constant regarding the surface material} \tag{16}$$

θ_p*: reference angle*

Here, θ is computed as

$$\theta = \cos^{-1}(-\vec{n} \cdot \vec{p}), \quad 0^\circ \le \theta \le 90^\circ. \tag{17}$$

This sinusoidal model for compensation was heuristically employed because it showed best performance in the various experiments.

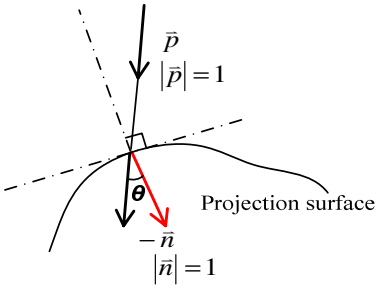

Fig. 5. Projection on nonplanar surface. θ represents the angle between two vectors. The intensity of projection per unit area is determined by θ.

The intensity of projection to the darker area is increased while the intensity of projection to the brighter area is decreased. Thus, the overall brightness of projection is similar to the brightness in the reference angle θ_p.

3 Experimental Results and Discussion

A projector (SONY VPL-CX6) and a camera (PointGrey Dragonfly) were used in our experiments. The images were at a resolution of 1024 by 768 pixels. An optical tracker (NDI Polaris) was used in the viewer-dependent projection.

Figure 6 shows the result of correcting the geometric distortion using the geometric registration method. After the projector was calibrated and the geometry of the cylindrical surface was recovered, the projection was prewarped to be undistorted.

Figure 7 shows the result of viewer-dependent projection. In the viewpoint of the projector, the projection is correct in Fig. 7-(b). However, the projection is wrong when considering the user's viewpoint. It was corrected and projected as shown in Fig. 7-(d) using the method explained in Section 2.3.

Fig. 6. Geometric distortion correction. Left image: before correction. Right image: after correction.

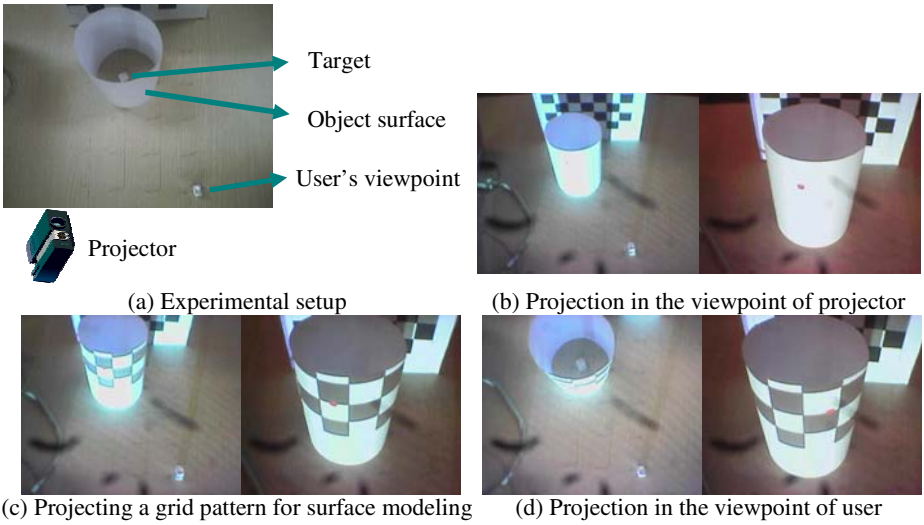

(a) Experimental setup (b) Projection in the viewpoint of projector

(c) Projecting a grid pattern for surface modeling (d) Projection in the viewpoint of user

Fig. 7. Viewer-dependent projection

For radiometric compensation, the geometry of projection surface was recovered using the geometric registration method first. To compute $\hat{V}$, four images were used in Fig. 8. The black image is required to estimate **F**. Let I_0, I_r, I_g, I_b be the pixel of each camera image, respectively. Then, the entries v_{ij} of $\hat{V}$ have the values as

$$v_{11} = v_{22} = v_{33} = 1.0,$$
$$v_{12} = (I_g(\mathrm{R})\text{-}I_0(\mathrm{R}))/(I_g(\mathrm{G})\text{-}I_0(\mathrm{G})),\ v_{13} = (I_b(\mathrm{R})\text{-}I_0(\mathrm{R}))/(I_b(\mathrm{B})\text{-}I_0(\mathrm{B})),$$
$$v_{21} = (I_r(\mathrm{G})\text{-}I_0(\mathrm{G}))/(I_r(\mathrm{R})\text{-}I_0(\mathrm{R})),\ v_{23} = (I_b(\mathrm{G})\text{-}I_0(\mathrm{G}))/(I_b(\mathrm{B})\text{-}I_0(\mathrm{B})),$$
$$v_{31} = (I_r(\mathrm{B})\text{-}I_0(\mathrm{B}))/(I_r(\mathrm{R})\text{-}I_0(\mathrm{R})),\ v_{32} = (I_g(\mathrm{B})\text{-}I_0(\mathrm{B}))/(I_g(\mathrm{G})\text{-}I_0(\mathrm{G})).$$

The channel-wise and pixel-wise response function of the projector was estimated from 26 projector input images with different values and their camera images as mentioned in Section 2.2. Figure 2 shows an example of the estimated projector response function of a point. The coefficients c_i (i=0,1,2,3,4) of the blue-channel response function were as follows.

$$c_0 = \text{-}27.6826,\ c_1 = 2.7801,\ c_2 = \text{-}0.0165,\ c_3 = 3.3769\text{e-}005,\ c_4 = 1.2253\text{e-}008$$

(a) Projector input image

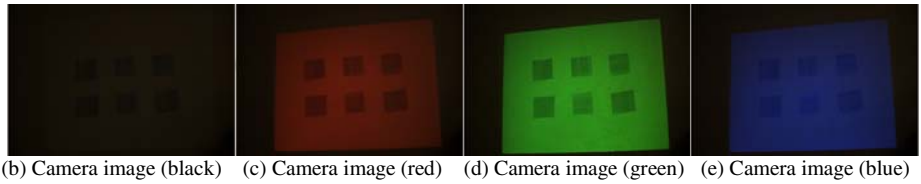

(b) Camera image (black) (c) Camera image (red) (d) Camera image (green) (e) Camera image (blue)

Fig. 8. Estimating the color mixing matrix $\hat{V}$

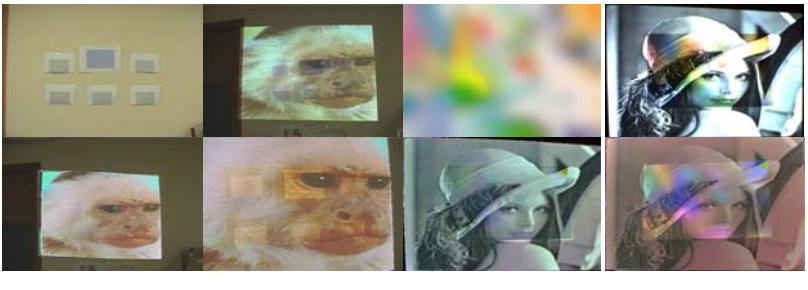

Fig. 9. Radiometric compensation. The right-top image shows that the projection color was distorted due to the texture of projection surface. There is no color distortion in the left-bottom image by compensating the projector input image. The right-bottom image shows the change of pixel values of projector input image for compensating the color distortion.

Fig. 10. Intensity-compensated projection. Left image: a projector lights the cylindrical surface on the left side and thus the left part of the image is brighter than the right part of the image. Right image: after compensation, the brightness of the whole image became similar.

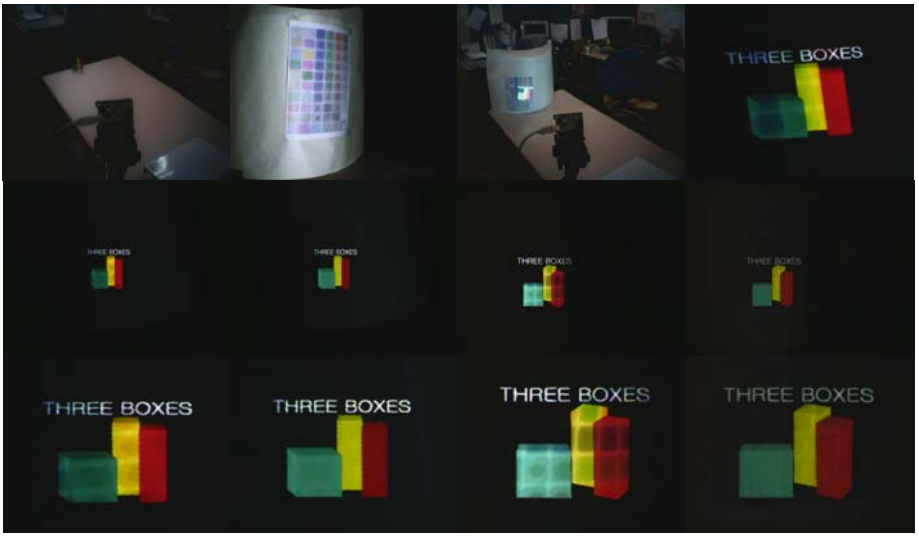

Fig. 11. Surface-independent direct-projected augmented reality. All the component methods are combined. First row: 3D target object (three blocks), nonplanar colored screen, without any compensation, magnification of the third image. Second row: after only geometric correction and after fully compensated projection when user's viewpoint is located on the left side of the screen, after only geometric correction and after fully compensated projection when user's viewpoint is located on the right side of the screen. Third row: magnification of the images of second row.

Figure 9 shows the result of compensating the color distortion using the radiometric compensation method. There is no color distortion in the left-bottom image of Fig. 9.

Figure 10 shows the result of intensity-compensated projection. The projector was calibrated and the geometry of the cylindrical surface was recovered. In the experiment, the brightness of the pixels within the red rectangle is the reference brightness and thus the brightness of the rest of the pixels was fit into the brightness.

The component methods for surface-independent DirectAR were combined to resolve mixed problems. The results are shown in Fig. 11.

4 Conclusion

A new framework for surface-independent DirectAR was presented. Various practical problems regarding DirectAR were addressed. Experimental results demonstrated that the problems unavoidable in realizing surface-independent DirectAR could be completely resolved using the proposed methods.

Currently, we are trying to develop an intelligent projection system using a single projector and apply to medical field. Developing an intelligent projection system using multiple projectors would be interesting as a future research.

Acknowledgement. This study was supported by a grant(02-PJ3-PG6-EV04-0003) of Ministry of Health and Welfare, Republic of Korea.

References

1. Grimson, W.E.L., etc.: An Automatic Registration Method for Frameless Stereotaxy, Image Guided Surgery, and Enhanced Reality Visualization. IEEE Transactions on Medical Imaging (1996)
2. Yasumuro, Y., Imura, M., Manabe, Y., Oshiro, O., Chihara, K.: Projection-Based Augmented Reality with Automated Shape Scanning. Proc. of SPIE EI (2005)
3. Snyder, J.M., Barr, A.H.: Ray Tracing Complex Models Containing Surface Tessellations. Proc. of SIGGRAPH, vol.21, no.4 (1987) 119-128
4. Grossberg, M.D., etc.: Making One Object Look Like Another: Controlling Appearance Using a Projector-Camera System. Proc. of CVPR (2004)
5. Hartley, R., Zisserman, A.: Multiple View Geometry. Cambridge University Press (2003)
6. Zhang, Z.: Flexible Camera Calibration by Viewing a Plane from Unknown Orientation. Proc. of ICCV (1999) 666-673
7. Surati, R.: Scalable Self-Calibrating Display Technology for Seamless Large-Scale Displays. PhD thesis, MIT (1999)
8. Raskar, R., etc.: iLamps: Geometrically Aware and Self-Configuring Projectors. Proc. of SIGGRAPH, vol.22 (2003) 809-818
9. NDI, http://www.ndigital.com/polaris.php
10. Mitsunaga T., etc.: Radiometric Self Calibration. Proc. of CVPR, vol.1 (1999) 374-380
11. Projector-related papers, http://www.cs.unc.edu/~raskar/Projector/projbib.html
12. Raskar, R., etc.: Shader Lamps: Animating Real Objects with Image-Based Illumination. Proc. of Eurographics Workshop on Rendering Techniques (2001) 89-102
13. Sukthankar, R., Stockton, R., Mullin, M.: Smarter Presentations: Exploiting Homography in Camera-Projector Systems. Proc. of ICCV (2001)
14. Bimber, O., Wetzstein, G., Emmerling, A., Nitschke, C.: Enabling View-Dependent Stereoscopic Projection in Real Environments. Proc. of ISMAR (2005) 14-23
15. Park, H., Lee, M.-H., Kim, S.-J., Park, J.-I.: Specular Reflection Elimination for Projection-Based Augmented Reality, Proc. of ISMAR (2005) 194-195